Title

Disentangling the Role of Surface Chemical Interactions on Interfacial Charge Transport at BiVO4 Photoanodes

Journal

ACS Applied Materials & Interfaces, 10(41)

ISSN

1944-8244

Authors

Eichhorn, Johanna

Kastl, Christoph

Schwartzberg, Adam M

et al.

Publication Date

2018-10-17

DOI

10.1021/acsami.8b11366

Peer reviewed

ACS APPLIED MATERIALS & INTERFACES

Energy, Environmental, and Catalysis Applications

Disentangling the role of surface chemical interactions on interfacial charge transport at BiVO photoanodes

Johanna Eichhorn, Christoph Kastl, Adam Michael Schwartzberg, Ian D. Sharp, and Francesca M. Toma

ACS Appl. Mater. Interfaces, **Just Accepted Manuscript** • DOI: 10.1021/acsami.8b11366 • Publication Date (Web): 19 Sep 2018

Just Accepted

ACS Publications

is published by the American Chemical Society. 1155 Sixteenth Street N.W., Washington, DC 20036

Disentangling the role of surface chemical interactions on interfacial charge transport at $BiVO_4$ photoanodes

Johanna Eichhorn[1], Christoph Kastl[2], Adam M. Schwartzberg[2], Ian D. Sharp[1,3], and Francesca M. Toma[1]*

[1] Chemical Sciences Division, Lawrence Berkeley National Laboratory, 1 Cyclotron Road, Berkeley, California 94720, USA.

[2] The Molecular Foundry, Lawrence Berkeley National Laboratory, 1 Cyclotron Road, Berkeley, California 94720, USA.

[3] Walter Schottky Institut and Physik Department, Technische Universität München, Am Coulombwall 4, 85748 Garching, Germany.

KEYWORDS: Interfaces, surface analysis, scanning probe microscopy, charge transfer, water splitting.

ABSTRACT

Chemical transformations that occur on photoactive materials, such as photoelectrochemical water splitting, are strongly influenced by the surface properties as well as by the surrounding environment. Herein, we elucidate the effects of oxygen and water surface adsorption on band alignment, interfacial charge transfer, and charge carrier transport by using complementary Kelvin probe measurements and photoconductive atomic force microscopy on bismuth vanadate. By observing variations in surface potential, we show that adsorbed oxygen acts as an electron trap state at the surface of bismuth vanadate, whereas adsorbed water results in formation of a dipole layer without inducing interfacial charge transfer. The apparent change of trap state density under dry or humid nitrogen, as well as under oxygen-rich atmosphere, proves that surface adsorbates influence charge carrier transport properties in the material. The finding that oxygen introduces electronically active states on the surface of bismuth vanadate may have important implications for understanding functional characteristics of water splitting photoanodes, devising strategies to passivate interfacial trap states, and elucidating important couplings between energetics and charge transport in reaction environments.

INTRODUCTION

Photoelectrochemical (PEC) water splitting has been gathering interest as a means to providing carbon neutral power and renewable fuels.[1,2] The chemical transformation of water into oxygen and hydrogen takes place at the surface of catalysts and photoactive materials. Consequently, the activity, efficiency, and reaction pathway are critically controlled by the surface properties of the material. Under PEC operating conditions, surface properties strongly depend on the surrounding

environment, and they may be altered in the course of the reaction. For example, during the water oxidation reaction, the oxygen concentration in the electrolyte increases and the generated oxygen can partially re-adsorb at the reaction interface.[3] The adsorbed molecules modify the chemistry at the surface, for example by influencing the kinetics of reactants, products, or reaction intermediates,[4] but they can also directly impact the electronic transport properties of the photoactive material by effectively acting as surface trap states. Photoanode materials, such as titania (TiO_2), bismuth vanadate ($BiVO_4$), or copper vanadate ($Cu_5V_2O_{10}$, $Cu_{11}V_6O_{26}$) are typically non-degenerate semiconductors, where surface states induce band bending, surface depletion, and Fermi level pinning.[5–8] These effects are even more relevant for nanostructured, thin film photoanodes, where the density of surface and interface states impacts the electronic transport, trapping, and recombination dynamics of (photogenerated) charge carriers. The charge transport through the bulk and the charge transfer at the surface are equally important factors governing the overall device performance and efficiency. Moreover, the photostability of the light absorber under operating conditions depends critically on the energy level alignment and charge transfer at the semiconductor surface.[9,10] Therefore, understanding the role of surface adsorbates, such as oxygen and water, on bulk charge transport and surface charge transfer processes is essential for the development of highly efficient light absorbers and integrated light absorber/catalyst systems, as well as for the development of effective passivation strategies for these materials.

In this work, we elucidate the influence of chemical interactions of adsorbed oxygen and water on charge transport and interfacial charge transfer of photogenerated charge carriers in polycrystalline $BiVO_4$ thin films. We choose monoclinic scheelite phase $BiVO_4$ due to its promising characteristics as a water splitting photoanode.[11–14] It has a moderate band gap,

favorable band alignment for water oxidation, relatively long charge carrier diffusion length, and it can yield high quantum efficiencies under water oxidation conditions.[11,13,15] Here, the charge transfer between adsorbates and $BiVO_4$ is monitored by Kelvin probe measurements under dry nitrogen, humid nitrogen, and oxygen environments at atmospheric pressure. To gain complementary insight into the relationship between surface interactions and interfacial charge transport characteristics, we employ photoconductive AFM (pc-AFM) under the respective environmental conditions. Recently, we have demonstrated for such thin film photoanodes that the low intrinsic bulk conductivity of $BiVO_4$ limits the electron transport through the film, and that the transport mechanism can be attributed to space charge limited current (SCLC) in the presence of trap states.[16] By combining these complementary techniques, we demonstrate that adsorbed oxygen acts as a surface trap state for electrons, which enhances the built-in potential and depletes the $BiVO_4$ layer, resulting in an increase of the measured surface photovoltage. By analyzing the SCLC, we estimate that the contribution of surface adsorbed oxygen to the total number of shallow traps is as large as 40%. For humid environments, our results are consistent with the adsorption of water as an oriented dipole layer, which does not induce a surface charge transfer but partially inhibits the adsorption of oxygen at the surface. Overall, environment-dependent analysis of the SCLC in combination with surface potential measurements on $BiVO_4$ provides detailed insights into the impact of surface adsorbates on the charge transport mechanism under *in-situ* conditions. Disentangling the individual effects of oxygen and water on surface band alignment and charge carrier trapping is important for optimizing photostability[10] and interfacial charge transfer, as well as for identifying limiting factors for the efficient transport of photogenerated charge carriers.

MATERIALS AND METHODS

Sample preparation. Undoped $BiVO_4$ thin films with a thickness of 60 nm were prepared by spin-coating on commercial fluorine-doped tin oxide (FTO) coated glass substrates following the procedure in Ref.[10] The crystal structure of the prepared $BiVO_4$ thin film and its purity is determined by X-ray diffraction as monoclinic scheelite phase.

Kelvin probe. Contact potential difference (CPD) was measured by Kelvin probe using a commercial Kelvin Probe S system and a Kelvin Control 07 (Besocke Delta Phi) under controlled environments. The Kelvin probe measurements were conducted using a piezoelectrically driven gold grid with a diameter of 3 mm. For all measurements, the sign convention of the measured CPD is $e\,\mathrm{CPD} = \phi_{\mathrm{BiVO_4}} - \phi_{\mathrm{Ref}}$, with the work functions of the metal reference electrode ϕ_{Ref} and the $BiVO_4$ thin film surface $\phi_{\mathrm{BiVO_4}}$. Prior to each measurement, samples were stored in the dark for at least 12 h. The Kelvin probe apparatus was combined with a closed gas cell. Three different environments were investigated: dry nitrogen, oxygen-rich (21% oxygen), and humid atmosphere (up to 40% RH). The oxygen concentration was monitored, and the residual concentration was better than the minimum reading of 0.5%. The humidity was controlled by adding water bubbled nitrogen to the gas flow. The variation of the CPD was studied in all three environments in the dark and under illumination. The samples were illuminated from the FTO-side using a CW-laser diode (405 nm) with a maximum light intensity of 140 mW cm^{-2}. The gas flow was kept constant during the measurements to ensure stable environmental conditions. All measurements were conducted at room temperature (24 °C). A stable CPD value was established in the dark over at least 2 h, and set to zero. Upon illumination, the CPD was allowed to settle to a new equilibrium value for at least 2 h depending

on the rate of equilibration. After the illumination cycle, CPD decay was monitored for at least 2 h.

JV-spectroscopy. *JV*-spectroscopy was performed with a commercial AFM system (Bruker Dimension Icon) under controlled environments. The $BiVO_4$ thin films were illuminated from the FTO-side as in Ref. [16]. A CW-laser diode laser (405 nm) was used as light source. The intensity was varied between 0 and 140 mW cm^{-2}. For all measurement, cantilevers with a nominal spring constant of 2.8 N m^{-1} or 0.5 N m^{-1} and a conductive metal coating of PtIr (Bruker SCM-PIT) or Au (MikroMasch HQ:NSC19/Cr-Au) were used. *JV*-spectroscopy was recorded by sweeping the sample bias from 0 to 3 V. At positive bias voltage, electrons are injected from the probe into the $BiVO_4$ thin film and are collected by the FTO back contact, similar to the operation conditions in a photoelectrochemical cell. Prior to all experiments, the AFM hood was purged with dry nitrogen atmosphere for several hours. The oxygen and humidity levels were monitored near the sample stage. The oxygen concentration was controlled by adding dry oxygen to the gas flow. The residual oxygen concentration was better than the minimum reading of 0.5%. The humidity was controlled by adding water bubbled nitrogen to the gas flow.

RESULTS AND DISCUSSION

Effect of adsorbed oxygen and water on surface potential of BiVO4 thin films.

We used nominally undoped, spin-coated $BiVO_4$ thin films on fluorine-doped tin oxide (FTO) coated glass substrates. As-synthesized $BiVO_4$ thin films have n-type character, which is typically attributed to the presence of oxygen vacancies[12] and/or hydrogen defects[17] that act as electron donors. To elucidate how adsorbates affect the surface potential and, consequently, the band bending of $BiVO_4$ thin films, we utilized Kelvin probe measurements under different

environmental conditions in dark and under illumination. Changes in the contact potential difference (CPD) between the sample and a reference electrode in the presence of adsorbates can be associated either with the formation of a polarized dipole layer[18,19] or with charge transfer between the substrate and the adsorbate[20,21]. While both of these processes can yield an increase or a decrease in the CPD, only the latter induces a change in the band bending and consequently in the surface photovoltage of the light absorber.

Figure 1 shows the time-resolved CPD measurements under dark conditions for different atmospheres. For all graphs, the equilibrium CPD in a dry nitrogen environment was set to ΔCPD = 0 V as the baseline. First, we studied the effect of water adsorption on the $BiVO_4$ surface (Figure 1a). Increasing the relative humidity (RH) to about 40% leads to a negative ΔCPD of about -27 mV. Calculations performed on $BiVO_4$ surfaces indicate that at room temperature molecular H_2O adsorption is favored over dissociative adsorption.[22,23] Upon molecular adsorption on the surface, water can create a dipole layer. First-principles molecular dynamics calculations on O-terminated (010) surfaces of $BiVO_4$ demonstrate that water molecules attach preferably to Bi sites.[22,24,25] In the presence of oxygen vacancies, the water molecule adsorbs at the V-Bi bridge site slightly tilted out of plane, with the O (negative polarization) pointing towards the Bi and the H (positive polarization) pointing away from the surface.[25] For such an orientation of the polar water molecule, the observed negative ΔCPD is consistent with the schematic orientation depicted in Figure 1b, with a negative charge polarization at the surface and a positive charge polarization away from the surface.[26] We note, that simulations of adsorption of atomic oxygen on $BiVO_4$ indicate that water and oxygen bind preferably to similar sites.[25] Then, in humid atmosphere, the ΔCPD could also be related to the replacement of previously adsorbed oxygen at the surface by water molecules (Figure 1b).[27,28]

This hypothesis is in agreement with CPD measurements performed when changing the environment from air to dry nitrogen (Figure S1), where a comparable behavior to humid atmosphere indicates that the process is dominated by water desorption from the surface.

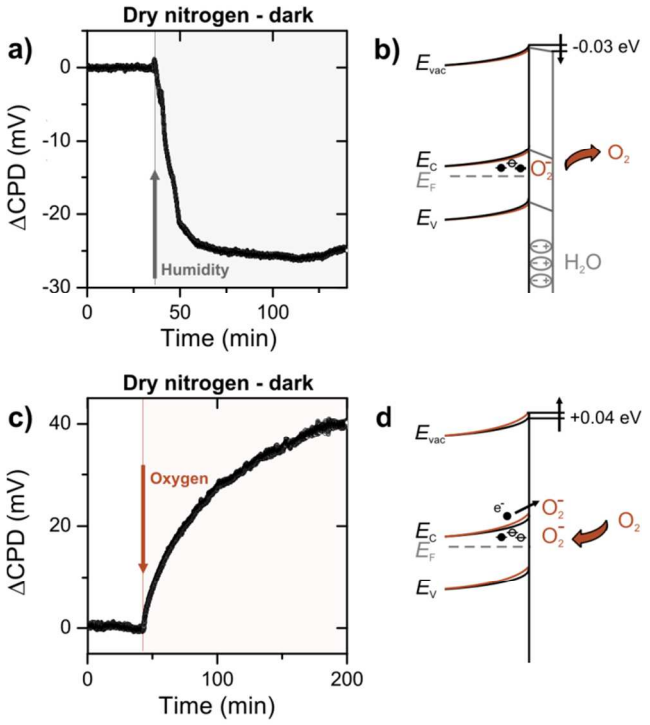

Figure 1. Oxygen and water adsorption on $BiVO_4$ in dark conditions. (a) Time-resolved contact potential difference (CPD) measurements after exposure to humidity. The baseline in dry nitrogen environment is set to zero. Upon increasing the relative humidity to about 40%, the equilibrium ΔCPD is about -27 mV. (b) Schematic band diagram with Fermi level, vacuum level (E_{vac}), conduction (E_c) and valence band (E_v). Non-dissociative water adsorption creates a dipole layer on the surface, and can lead to a reduced surface concentration of oxygen as a consequence of competitive adsorption/desorption events (red arrow). (c) CPD measurement after exposure to oxygen. An increase of the oxygen concentration to 21% yields a ΔCPD of about +40 mV. (d) Schematic illustration of the electron charge transfer from the surface of $BiVO_4$ to O_2, which

results in chemisorption of O_2^- (brown arrow), thus increasing the band bending (brown lines) compared to dry nitrogen environment (black lines).

In Figure 1c, increasing the oxygen concentration to 21% resulted in a positive ΔCPD = +40 mV. While oxygen adsorption at the $BiVO_4$ surface has been rarely studied, there exists previous reports that detail the adsorption of oxygen on other metal oxide semiconductors surfaces such as TiO_2 and SnO_2. In these cases, charge transfer from the semiconductor to the oxygen molecules leads to the chemisorption of negatively charged oxygen molecules O_2^- the surface, thereby increasing the surface potential.[21,29,30] This picture is in agreement with the positive ΔCPD for changing the environment from dry nitrogen to 21% oxygen under dark conditions (Figure 1c). The negatively charged oxygen ions lead to a corresponding increase of the band bending (Figure 1d). In this scenario, the oxygen acts as a surface trap state that can effectively deplete $BiVO_4$, which in turn can influence the interfacial charge transport properties.

In order to provide insights on photoinduced changes of the band bending in the presence of adsorbates, we studied the surface charge transfer dynamics with above band gap illumination (E_{ph} = 3.06 eV) by measuring the time-dependent CPD in different environments (Figure 2). The measurement cycle is described as follows. Initially, a stable baseline value of the CPD was established in the dark, and the resulting value was set to 0 V. Then, the illumination was switched on, and the CPD was allowed to settle to a new value representing the steady state condition. Finally, the illumination was ceased and the evolution back to equilibrium was traced. In oxygen environment (Figure 2a), illumination results in a drop of the CPD in less than a minute by ΔCPD = -0.16 ± 0.03 V upon illumination. Then, ΔCPD is partially compensated over several hours to a steady state value of -0.06 ± 0.02 V. Finally, when the illumination is turned

off, the CPD returns to the baseline value within about 10 min. The behavior during this cycle can be understood as follows. Upon excitation, photogenerated electrons and holes are separated by the internal electric field in the depletion region. Holes accumulate at the surface, while electrons drift to the bulk or occupy localized states, *e.g.* shallow defects, near the surface.[31] This charge separation immediately gives rise to a photovoltage, which partially accounts for the initial ΔCPD. Furthermore, photogenerated holes can recombine with electrons trapped by adsorbed oxygen, and stimulate oxygen desorption.[32] This process contributes to reduce the surface potential under illumination. Therefore, we assign the initial ΔCPD to both the separation of photogenerated charge carriers and the desorption of oxygen stimulated by photogenerated holes. In addition, as detailed in the next sections, the slow compensation of ΔCPD for prolonged illumination is ascribed to desorption of water from previous exposure to humidity.

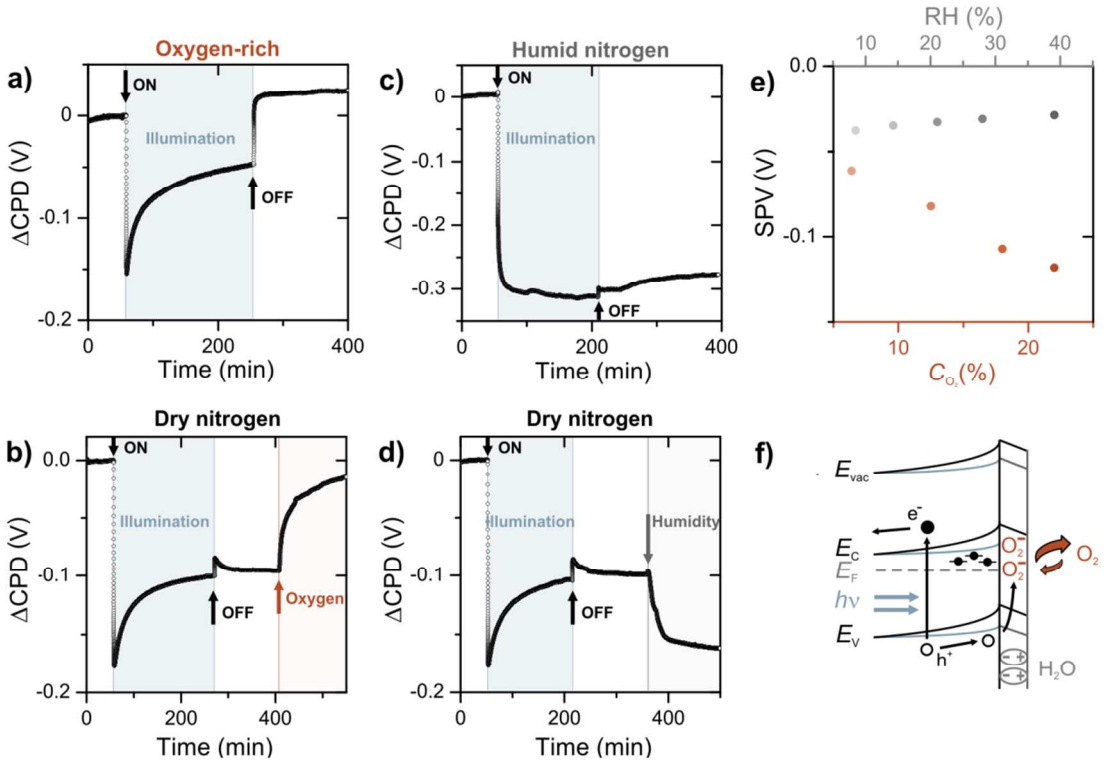

Figure 2. Effect of environment on surface potential and photovoltage under illumination. Time-resolved CPD measurements in oxygen-rich (a), dry nitrogen (b,d), and humid nitrogen (c) environment for a single illumination cycle. For each measurement the equilibrium CPD in the dark is used as a baseline and set to zero. Under illumination, the negative ΔCPD in all environments indicate a decreased band bending. As the illumination is turned off, the CPD is reversed to its original value in oxygen-rich environment (a), whereas the CPD persists in dry nitrogen and humid nitrogen (b, c, d). The CPD is fully reversed to the value before illumination by dosing oxygen in dry nitrogen atmosphere (b). (e) Surface photovoltage (SPV) for increasing oxygen concentration and increasing relative humidity. (f) Schematic illustration of the oxygen desorption/adsorption processes and the water dipole layer under illumination. The band edges in dark (under illumination) are shown in black (blue). Under illumination, electron–hole pairs are generated and separated by the built-in field, which gives rise to a surface photovoltage.

Switching off the illumination leads to a fast increase of the CPD close to the initial baseline value in oxygen-rich environment (Figure 2a). The first step in the decay process is fast recombination of free photogenerated electrons and holes. In the second step, electrons captured in localized shallow defects have to transfer to empty surface states to restore dark conditions. Oxygen adsorption provides an efficient pathway to capture electrons from the $BiVO_4$ film, effectively restoring the initial CPD.

In dry nitrogen, a similar response to the one in oxygen-rich environment is observed under illumination, with a slightly increased initial drop of ΔCPD = -0.20 ± 0.04 V (Figure 2b). Upon switching off the illumination, the fast increase of the CPD is reduced to about ΔCPD = +14 ± 4.9 mV compared to oxygen-rich environment. Furthermore, the CPD remains close to the

steady-state value under illumination. However, the baseline value can be fully recovered upon subsequent exposure to oxygen in the dark (Figure 2b). These results suggest that the increased initial ΔCPD under illumination and the ΔCPD value after illumination are due to net photodesorption of oxygen from previous exposure to air.

Additional measurements in humid environment (40% RH) show different dynamic behavior compared to oxygen-rich and dry nitrogen environment (Figure 2c). Upon illumination, we find that the CPD has a fast decay of ΔCPD ≈ -0.16 V followed by a slow continued decrease to an equilibrium value ΔCPD = -0.26 ± 0.05 V. The timescale and the sign of the latter process are consistent with the water adsorption measured in Figure 1a. We note that the previously discussed photodesorption of oxygen from the surface may result in an enhanced adsorption of water, which can explain the large magnitude of the observed ΔCPD in humid environment. Conversely in dry oxygen (Figure 2a) and nitrogen (Figure 2b) atmosphere, the slow compensation process under illumination may be associated with photostimulated desorption of water from previous exposure to atmosphere. To test this hypothesis, we performed an illumination cycle in dry nitrogen, with subsequent dosing of humid nitrogen after illumination (Figure 2d). The exposure to humidity under dark conditions promotes re-adsorption of water and decreases the CPD, which supports the hypothesis of water desorption under prolonged illumination.

The ΔCPD after illumination indicates that the surface photovoltage (SPV) and the built-in potential are significantly increased by the presence of oxygen. Figures S2 show a series of fast illumination cycles (30 s illumination on, 30 s illumination off) under various oxygen and water concentrations. In these conditions, the desorption/adsorption of oxygen and water processes appear quasi-static, and the difference between the on- and off-state can be interpreted as the

SPV. We find that the SPV increases with oxygen concentration, whereas it is almost independent of water concentration (Figures 2e). This result confirms that oxygen adsorption at the $BiVO_4$ surface involves a charge transfer step. Therefore, oxygen adsorption effectively acts as a surface trap state that increases the band bending. By contrast, water adsorption does not significantly modify the SPV; rather, it adsorbs as a dipolar layer that affects the CPD without a charge transfer step at the $BiVO_4$ surface. Figure 2f summarizes schematically the adsorption and charge transfer processes under illumination.

Effect of adsorbed oxygen and water on charge transport properties of $BiVO_4$ films.

While Kelvin probe provides direct insights into the interplay of photoinduced charge transfer, band alignment, and surface adsorbates, photoconductive AFM (pc-AFM) provides information about how photogenerated charge carriers contribute to the electronic transport in the material.[16] With pc-AFM, complementary single current-voltage curves (*JV*-curves) and (photo)current maps can be recorded, thus revealing the charge transport mechanism and nanoscale (opto)electronic heterogeneity, respectively. *JV*-curves were recorded in the dark and under illumination for increasing oxygen concentrations, as well as for increasing RH values in dry nitrogen environment (Figure 3). In agreement with a previous study,[16] the *JV*-curves are best described by a power law relation ($J \propto V^m$) for high sample biases ($V_s > 0.7$ V) independent of the exact environmental conditions, which is characteristic for SCLC as the dominant charge transport mechanism. In the SCLC model, a power law exponent of $m = 2$ describes the charge transport in ideal trap-free materials. In the presence of trap states, the SCLC follows a modified power law with $m > 2$. In a log-log plot, the slope of the *JV*-curves corresponds to the power law

exponent m, which is also related to the characteristic energy of the trap states E_t with respect to the band edge by $m = 1 + E_t/(k_B T)$.

For increasing oxygen concentrations, the *JV*-curves show a decrease in current by more than one order of magnitude and larger slope (higher m) in the dark as well as under illumination (Figure 3a and 3b). Under dark conditions, the power law increases from $m = 3.6$ in dry nitrogen to $m = 5.1$ in oxygen-rich (21%) environment (Figure 3a), thus indicating a stronger influence of trap states on charge transport in the presence of oxygen. The calculated characteristic energy of trap states indicates shallow defect states, with a characteristic energy $E_t = 0.07$ eV in dry nitrogen environment compared $E_t = 0.11$ eV in oxygen-rich ambient. Adsorbed oxygen provides additional surface traps, which compete with the trap state filling in the bulk. Therefore, higher oxygen concentrations and increased oxygen adsorption at the $BiVO_4$ surface effectively reduce the free electron concentration in the near surface region, due to increased surface trapping and subsequently reduced trap state filling in the material. This behavior is reflected by the increase of the power law exponent m as well as by the characteristic energy E_t under oxygen-rich environment with respect to dry nitrogen in the dark. Under dry nitrogen conditions, the effective trap state filling is higher and consequently the power law exponent of SCLC is closer to $m = 2$, which corresponds to a trap-free material. Under illumination, the environment dependence of the *JV*-curves is similar to dark conditions, and oxygen absorption leads to enhanced trapping with $m = 2.6$ ($E_t = 0.04$ eV) in nitrogen and $m = 4.0$ ($E_t = 0.08$ eV) in oxygen (Figure 3b). Overall, the power law exponent is decreased due to trap state filling by photogenerated charge carriers.[16]

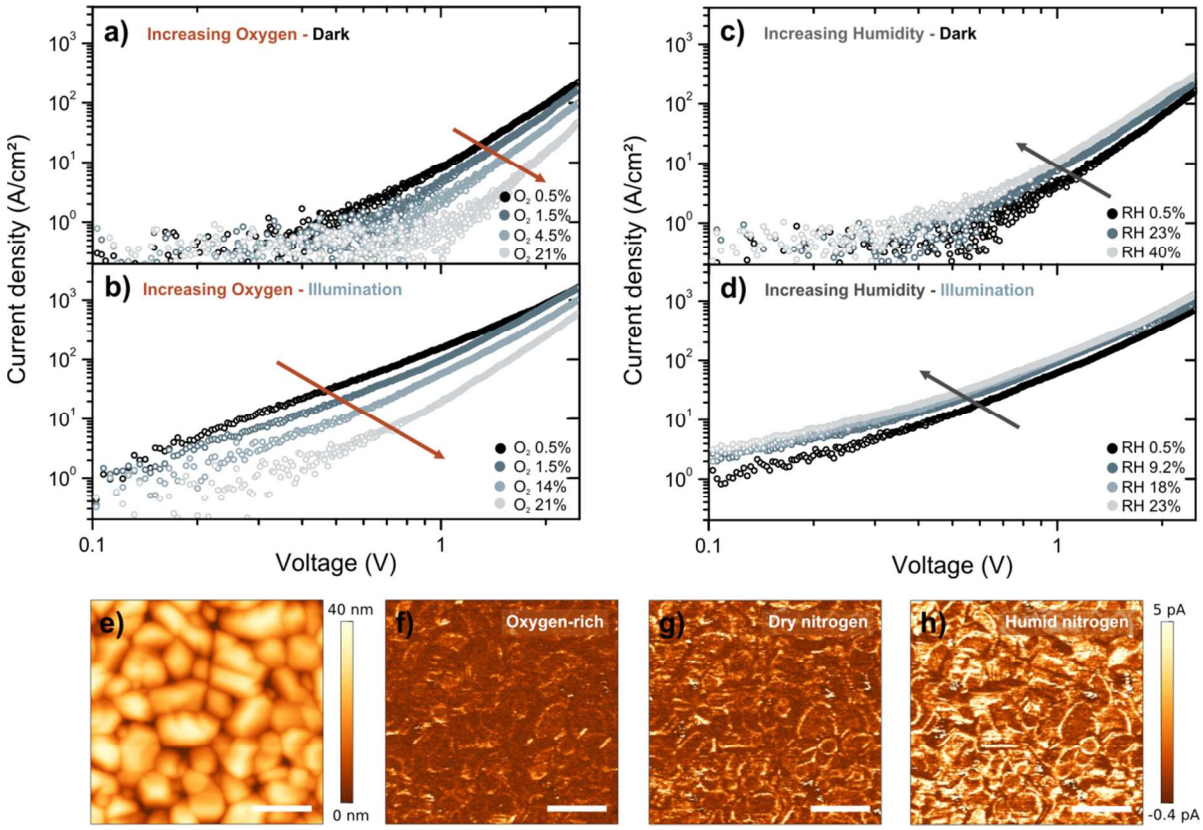

Figure 3. Effect of different environments on electronic transport. *JV*-characteristics of the FTO/$BiVO_4$/probe circuit for increasing oxygen concentration in the dark (a) and under illumination (b). The curves follow approximately $J \propto V^m$, *i.e.* a linear relation of log(*J*) and log(*V*), which is attributed to a space charge limited transport mechanism in the presence of trap states. The increase of the slope with oxygen concentration indicates enhanced charge trapping. *JV*-characteristics for increasing relative humidity show constant slope in the dark (c) and under illumination (d). (e) Topography and current images of under illumination (V_s = 1.75 V) in oxygen (f), dry (g), and humid (h) nitrogen atmosphere measured at identical areas. The maps are acquired at the same area on the sample. The current increases in the order oxygen, dry nitrogen and humid nitrogen environment, whereas the overall image contrast stays the same. Scale bars are 200 nm.

For increasing relative humidity (Figures 3c and 3d), the *JV*-curves show slightly increased current, which is opposite to the behavior observed for oxygen-rich environment. Under dark conditions, the power law exponent slightly changes from $m = 4.3$ ($E_t = 0.08$ eV) in dry nitrogen to $m = 3.7$ ($E_t = 0.07$ eV) in 40% relative humidity. This is consistent with the CPD measurements, where we found that water does not directly introduce surface trap states. The apparent increase in conductivity may be related to the replacement of residual oxygen with water molecules on the surface of $BiVO_4$. Furthermore, the water dipole layer may affect the energetic alignment between the surface and the probe, and, as a consequence, the injected current.

Under illumination (Figure 3d), the power law exponent is significantly lowered and constant at $m = 2.45 \pm 0.05$ ($E_t = 0.04$ eV) independent of the relative humidity. This result points towards net photodesorption of residual oxygen under illumination in both dry nitrogen and humid environment compared to the oxygen-rich case. Similar behavior was reported in previous studies, which attributed photoconductivity in ZnO to oxygen desorption for relative humidities below 60%.[27] Accordingly, water adsorption only indirectly influences the charge transport in $BiVO_4$ by removing surface adsorbed oxygen. Furthermore, the weak dependence of conductivity on water concentration supports the hypothesis that water adsorption on the $BiVO_4$ surface occurs by dipole formation without net charge transfer to $BiVO_4$.

As discussed above, Kelvin probe measurements revealed a constant ΔCPD (Figure 2) after illumination in dry nitrogen and humid atmospheres, when the sample was previously exposed to oxygen. We attributed this to removal of residual surface adsorbed oxygen during illumination. This effect is consistent with the fact that we observe a persistent enhancement of conductivity in dry nitrogen and humid environments after illumination, which is less pronounced with respect

to the oxygen-rich environment (Figure S3). In dry and humid nitrogen atmospheres, the photo-enhancement of conductivity persists almost unaltered after switching off the illumination. The effect is almost completely compensated upon exposure to oxygen.

The *JV*-characteristics of SCLC are extremely sensitive to the presence of surface adsorbates that can trap charge carriers. We further leverage this sensitivity to determine the trap state density in $BiVO_4$ in oxygen-rich and dry nitrogen environments, which is effectively given by the combination of adsorbate induced trap states at the surface and intrinsic trap states in the material. For this purpose, we measured *JV*-curves as a function of sample temperature (Figure 4) and light intensity (Figure S4) in both environments. The log-log slope converges towards $m = 2$ with increasing temperatures, and we fitted a power law relation for $V_s > 0.7$ V. The extrapolated *JV*-curves intersect at a crossover voltage $V_c = 5.6$ in oxygen and $V_c = 3.5$ in nitrogen. The crossover is characteristic for the SCLC model with traps and is directly related to the trap density $H_t = \frac{2V_c \cdot \epsilon_0 \epsilon_r}{qd^2}$ with the thickness d and the dielectric permittivity ϵ_r of the $BiVO_4$ film. With the value of the $BiVO_4$ film thickness d = 60 nm and assuming a dielectric constant $\epsilon_r = 52$,[10] we can calculate the apparent trap density to be $H_t = 8.9\ 10^{18}$ cm^{-3} in oxygen-rich environment and $H_t = 5.6\ 10^{18}$ cm^{-3} in dry nitrogen environment. Therefore, we surmise that the effective trap state density, which considers the trap density in the material and at the surface, is reduced by about 40% by changing the environment from oxygen-rich to dry nitrogen due to the removal of adsorbed oxygen, which is acting as a surface trap state for electrons.

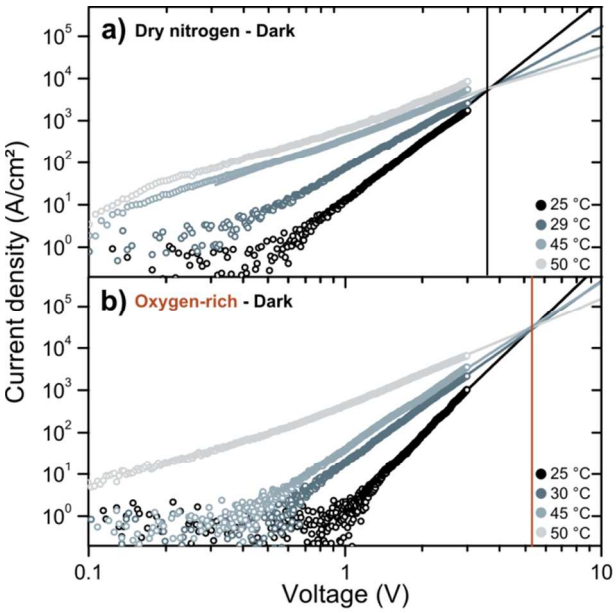

Figure 4. Trap state density in dry nitrogen and oxygen-rich ambient. *JV*-characteristics of the FTO/$BiVO_4$/probe circuit in dry nitrogen (a) and oxygen-rich ambient (b) for varying temperature under dark conditions. In the SCLC model with trap states, the crossover voltage is proportional to the trap state density. Solid lines are power law fits to the data intersecting at different crossover voltage V_c corresponding to effective trap densities of $8.9 \cdot 10^{18}$ cm^{-3} (oxygen) and $5.6 \cdot 10^{18}$ cm^{-3} (nitrogen).

CONCLUSION

By combining contact potential measurements and current-voltage spectroscopy, we revealed the effect of oxygen and water adsorption on the surface potential and electronic transport in $BiVO_4$ thin films. For adsorbed oxygen, we find an increased surface potential, increased photovoltage and an enhanced contribution of trap states to transport, which decreases the conductivity. Our results suggest that chemisorbed oxygen acts as a surface trap state for

electrons, thereby depleting the $BiVO_4$ *via* interfacial charge transfer and inducing upwards surface band bending. Water absorption instead decreases the surface potential without affecting the photovoltage, which we assign to the formation of a dipole layer without an interfacial charge transfer. Under above band gap illumination, we describe the dynamics of the surface potential by the competing effects of photoinduced oxygen desorption and water adsorption. We observe a persistent enhancement of conductivity and decrease of the CPD in oxygen depleted atmosphere (dry nitrogen and humid atmosphere), which is reversible upon exposure to oxygen in the dark and can be ascribed to photodesorption of residual oxygen from previous exposure to air. Furthermore, we describe the transport by a space charge limited model with trap states to quantify the effective trap state density in different environments. The apparent trap state density is reduced by 40% in dry nitrogen ambient compared to oxygen-rich ambient highlighting the strong influence of surface adsorbed oxygen on charge carrier trapping. Our study underpins the importance of trap state passivation to improve charge carrier transport in $BiVO_4$. Furthermore, this work motivates future *operando* studies of $BiVO_4$ photoanodes by suggesting that photoelectrochemical generation of oxygen could simultaneously impact surface state distributions, energetics, and charge transport. Improved understanding of these complex interactions will aid the development and integration of effective passivation and catalyst layers.

ASSOCIATED CONTENT

Supporting Information. Supporting Information contains additional supporting measurements of surface potential, statistical analysis on photocurrent distribution, and additional supporting *JV*-characteristics. Supplementary Dataset includes all the data source for figures 1a and c, 2a-e, 3a-d, 4a-b.

AUTHOR INFORMATION

Corresponding Author

*E-mail: fmtoma@lbl.gov

Author Contributions

The manuscript was written through contributions of all authors. All authors have given approval to the final version of the manuscript.

Funding Sources

Laboratory Directed Research and Development Program of Lawrence Berkeley National Laboratory under U.S. Department of Energy contract number DE-AC02-05CH11231.

Notes

The authors declare no competing financial interest.

ACKNOWLEDGMENT

This study was supported by the Laboratory Directed Research and Development Program of Lawrence Berkeley National Laboratory under U.S. Department of Energy contract number DE-AC02-05CH11231. The use of the Molecular Foundry was supported by the Office of Science, Office of Basic Energy Sciences, of the U.S. Department of Energy under contract number DE-AC02-05CH11231 is gratefully acknowledged.

ABBREVIATIONS

PEC, photoelectrochemical; TiO_2, titania; $BiVO_4$, bismuth vanadate; pc-AFM, photoconductive AFM; SCLC, space charge limited current; FTO, fluorine-doped tin oxide; CPD, contact potential difference; RH, relative humidity; E_{vac}, vacuum level; E_c, conduction; E_v, valence band (E_v); SPV, surface photovoltage; *JV, c*urrent-voltage.

REFERENCES

(1) Van de Krol, R.; Grätzel, M. *Photoelectrochemical Hydrogen Production*; Springer, 2012; Vol. 90.

(2) Lewis, N. S.; Nocera, D. G. Powering the Planet: Chemical Challenges in Solar Energy Utilization. *Proc. Natl. Acad. Sci.* **2006**, *103*, 15729–15735.

(3) Wang, J.; Liu, T.; Dong, J.; Li, M.; He, J.; Jiang, C. Vertical Charge Transport via Small Polaron Hopping within TIPS-Pentacene Lamellar Single Crystal. *Small* **2017**, *13*, 1700456.

(4) Kuo, D.-Y.; Eom, C. J.; Kawasaki, J. K.; Petretto, G.; Nelson, J. N.; Hautier, G.; Crumlin, E. J.; Shen, K. M.; Schlom, D. G.; Suntivich, J. Influence of Strain on the Surface–Oxygen Interaction and the Oxygen Evolution Reaction of $SrIrO_3$. *J. Phys. Chem. C* **2018**, *122*, 4359–4364.

(5) Trześniewski, B. J.; Smith, W. A. Photocharged $BiVO_4$ Photoanodes for Improved Solar Water Splitting. *J Mater Chem A* **2016**, *4*, 2919–2926.

(6) Jiang, C.-M.; Segev, G.; Hess, L. H.; Liu, G.; Zaborski, G.; Toma, F. M.; Cooper, J. K.; Sharp, I. D. Understanding Energy Conversion and Loss Mechanisms in Ternary Metal Oxide Photoelectrodes: The Case of Copper Vanadate. **2017**, DOI:10.26434/chemrxiv.5514871.v1.

(7) Chang, X.; Wang, T.; Zhang, P.; Zhang, J.; Li, A.; Gong, J. Enhanced Surface Reaction Kinetics and Charge Separation of p–n Heterojunction Co_3O_4/$BiVO_4$ Photoanodes. *J. Am. Chem. Soc.* **2015**, *137*, 8356–8359.

(8) Dang, K.; Chang, X.; Wang, T.; Gong, J. Enhancement of Photoelectrochemical Oxidation by an Amorphous Nickel Boride Catalyst on Porous $BiVO_4$. *Nanoscale* **2017**, *9*, 16133–16137.

(9) Eichhorn, J.; Liu, G.; Toma, F. M. Degradation of Semiconductor Electrodes in Photoelectrochemical Devices: Principles and Case Studies, In *Integrated Solar Fuel Generators*; Atwater, H. A., Lewerenz, A., Sharp. I. D., RSC Publishing **2018,** *in press*.

(10) Toma, F. M.; Cooper, J. K.; Kunzelmann, V.; McDowell, M. T.; Yu, J.; Larson, D. M.; Borys, N. J.; Abelyan, C.; Beeman, J. W.; Yu, K. M.; Yu, K. M.; Yang, J.; Chen, L.; Shanner, M. R.; Spurgeon, J.; Houle, F. A.; Persson, K. A.; Sharp, I. D. Mechanistic Insights into Chemical and Photochemical Transformations of Bismuth Vanadate Photoanodes. *Nat. Commun.* **2016**, *7*, 12012.

(11) Kudo, A.; Ueda, K.; Kato, H.; Mikami, I. Photocatalytic O_2 Evolution under Visible Light Irradiation on $BiVO_4$ in Aqueous $AgNO_3$ Solution. *Catal. Lett.* **1998**, *53*, 229–230.

(12) Kim, T. W.; Choi, K.-S. Nanoporous $BiVO_4$ Photoanodes with Dual-Layer Oxygen Evolution Catalysts for Solar Water Splitting. *Science* **2014**, *343*, 990–994.

(13) Sharp, I. D.; Cooper, J. K.; Toma, F. M.; Buonsanti, R. Bismuth Vanadate as a Platform for Accelerating Discovery and Development of Complex Transition-Metal Oxide Photoanodes. *ACS Energy Lett.* **2016**, *2*, 139–150.

(14) Park, Y.; McDonald, K. J.; Choi, K.-S. Progress in Bismuth Vanadate Photoanodes for Use in Solar Water Oxidation. *Chem Soc Rev* **2013**, *42*, 2321–2337.

(15) Abdi, F. F.; Savenije, T. J.; May, M. M.; Dam, B.; van de Krol, R. The Origin of Slow Carrier Transport in $BiVO_4$ Thin Film Photoanodes: A Time-Resolved Microwave Conductivity Study. *J. Phys. Chem. Lett.* **2013**, *4*, 2752–2757.

(16) Eichhorn, J.; Kastl, C.; Cooper, J. K.; Ziegler, D.; Schwartzberg, A. M.; Sharp, I. D. Nanoscale Imaging of Charge Carrier Transport in Water Splitting Photoanodes. *Nat. Commun.* **2018**, *9*, 2597.

(17) Cooper, J. K.; Scott, S. B.; Ling, Y.; Yang, J.; Hao, S.; Li, Y.; Toma, F. M.; Stutzmann, M.; Lakshmi, K. V.; Sharp, I. D. The Role of Hydrogen in Defining the n-Type Character of $BiVO_4$ Photoanodes. *Chem. Mater.* **2016**, *28*, 5761–5771.

(18) Sugimura, H.; Ishida, Y.; Hayashi, K.; Takai, O.; Nakagiri, N. Potential Shielding by the Surface Water Layer in Kelvin Probe Force Microscopy. *Appl. Phys. Lett.* **2002**, *80*, 1459–1461.

(19) Rühle, S.; Cahen, D. Contact-Free Photovoltage Measurements of Photoabsorbers Using a Kelvin Probe. *J. Appl. Phys.* **2004**, *96*, 1556–1562.

(20) Burshtein, R. K.; Shurmovskaya, N. A. Effect of Chemisorbed Gasses on the Work Function of Metals. *Russ. Chem. Rev.* **1965**, *34*, 746–751.

(21) Sahm, T.; Gurlo, A.; Bârsan, N.; Weimar, U. Basics of Oxygen and SnO_2 Interaction; Work Function Change and Conductivity Measurements. *Sens. Actuators B Chem.* **2006**, *118*, 78–83.

(22) Oshikiri, M.; Boero, M. Water Molecule Adsorption Properties on the $BiVO_4$ (100) Surface. *J. Phys. Chem. B* **2006**, *110*, 9188–9194.

(23) Yang, J.; Wang, D.; Zhou, X.; Li, C. A Theoretical Study on the Mechanism of Photocatalytic Oxygen Evolution on $BiVO_4$ in Aqueous Solution. *Chem. – Eur. J.* **2013**, *19*, 1320–1326.

(24) Crespo-Otero, R.; Walsh, A. Variation in Surface Ionization Potentials of Pristine and Hydrated $BiVO_4$. *J. Phys. Chem. Lett.* **2015**, *6*, 2379–2383.

(25) Hu, J.; Zhao, X.; Chen, W.; Su, H.; Chen, Z. Theoretical Insight into the Mechanism of Photoelectrochemical Oxygen Evolution Reaction on $BiVO_4$ Anode with Oxygen Vacancy. *J. Phys. Chem. C* **2017**, *121*, 18702–18709.

(26) Leung, T. C.; Kao, C. L.; Su, W. S.; Feng, Y. J.; Chan, C. T. Relationship between Surface Dipole, Work Function and Charge Transfer: Some Exceptions to an Established Rule. *Phys. Rev. B* **2003**, *68*, 195408.

(27) Li, Y.; Della Valle, F.; Simonnet, M.; Yamada, I.; Delaunay, J.-J. Competitive Surface Effects of Oxygen and Water on UV Photoresponse of ZnO Nanowires. *Appl. Phys. Lett.* **2009**, *94*, 023110.

(28) Liu, Y.-J.; Zhang, H.-D.; Zhang, J.; Li, S.; Zhang, J.-C.; Zhu, J.-W.; Gong, M.-G.; Wang, X.-X.; Long, Y.-Z. Effects of Ce Doping and Humidity on UV Sensing Properties of Electrospun ZnO Nanofibers. *J. Appl. Phys.* **2017**, *122*, 105102.

(29) Bârsan, N.; Hübner, M.; Weimar, U. Conduction Mechanisms in SnO2 Based Polycrystalline Thick Film Gas Sensors Exposed to CO and H_2 in Different Oxygen Backgrounds. *Sens. Actuators B Chem.* **2011**, *157*, 510–517.

(30) Petrik, N. G.; Kimmel, G. A.; Shen, M.; Henderson, M. A. Quenching of Electron Transfer Reactions through Coadsorption: A Study of Oxygen Photodesorption from TiO_2 (110). *Surf. Sci.* **2016**, *652*, 183–188.

(31) Winnerl, A.; Pereira, R. N.; Stutzmann, M. Kinetics of Optically Excited Charge Carriers at the GaN Surface. *Phys. Rev. B* **2015**, *91*, 075316.

(32) Bao, J.; Shalish, I.; Su, Z.; Gurwitz, R.; Capasso, F.; Wang, X.; Ren, Z. Photoinduced Oxygen Release and Persistent Photoconductivity in ZnO Nanowires. *Nanoscale Res. Lett.* **2011**, *6*, 404.

TOC